Bitlis Eren Üniversitesi Fen Bilimleri Dergisi
BİTLİS EREN UNIVERSITY JOURNAL OF SCIENCE
ISSN: 2147-3129/e-ISSN: 2147-3188
VOLUME: 13 NO: 4 PAGE: 1304-1313 YEAR: 2024
DOI: 10.17798/bitlisfen.1558069

SimCLR-based Self-Supervised Learning Approach for Limited Brain MRI and Unlabeled Images

Kazım FIRILDAK[1*], Gaffari ÇELİK[2], Muhammed Fatih TALU[3]
[1]*Firat University, Department of Computer Technology, Elazığ, Türkiye*
[2]*Ağrı İbrahim Çeçen University, Department of Computer Technology, Ağrı, Türkiye*
[3]*İnönü University, Department of Computer Science, Malatya, Türkiye*
(ORCID: 0000-0002-1958-3627) (ORCID: 0000-0001-5658-9529) (ORCID: 0000-0003-1166-8404)

Keywords: Unlabeled images, Brain tumor, Self-Supervised learning, SimCLR, Barlow twins, NnCLR

Abstract
In this study, a SimCLR-based model is proposed for the classification of unlabeled brain tumor images in medical imaging using a self-supervised learning (SSL) technique. Additionally, the performances of different SSL techniques (Barlow Twins, NnCLR, and SimCLR) are analyzed to evaluate the performance of the proposed model. Three different datasets, consisting of pituitary, meningioma, and glioma brain tumors as well as non-tumor images, were used as the dataset. Out of a total of 7,671 images, 6,128 were used as unlabeled data, and the model was trained with both labeled and unlabeled data. The proposed model achieved high performance with unlabeled data, reducing the need for manual labeling. As a result, the model demonstrated superior performance compared to other models, with high performance values such as 99.35% c_acc and 96.31% p_acc.

1. Introduction

Deep learning has become a widely used method in image classification [1],[2],[3], segmentation [4],[5],[6], audio processing [7],[8],[9], object detection [10],[11], and natural language processing (NLP) [12],[13] tasks. Significant improvements have been achieved, especially in challenging areas such as disease classification and organ segmentation in medical image analysis. These successes are often based on large amounts of manually labeled training data. While labels can be easily obtained through crowd sourcing in natural images, this method is limited in medical imaging due to the requirement of expert knowledge. This situation indicates that access to unlabeled medical images is often easier than access to labeled images [14].

Supervised learning approaches have reached their limits due to the challenges and costs associated with the manual annotation of labeled data. Additionally, image recognition systems learn image representations using large amounts of images along with semantic annotations for these images. These annotations can be provided in different formats such as class labels, hashtags, or bounding boxes. However, predefined semantic annotations often fail to encompass the long tail of diverse and rare visual concepts. This limitation hinders progress in the performance of image recognition systems [15],[16],[17].

While traditional methods rely on annotations in large datasets, self-supervised methods enable more efficient use of deep learning by providing the ability to learn without the need for these annotations. These methods further advance developments in the field of deep learning by facilitating feature learning from unlabeled data [15],[18].

Self-supervised learning (SSL) is defined as a learning paradigm that sits between unsupervised learning and supervised learning. Compared to supervised learning, it aims to learn without the requirement for labeled data. Instead, it allows the model to generate labels for itself by leveraging the natural structure and relationships within the data. In this way, the model extracts “supervisory signals” from the data itself. In supervised learning approaches, large amounts of labeled data are generally required for the model to learn. However, this labeling process can be time-consuming and costly. SSL aims to learn by utilizing the intrinsic

*Corresponding author: kfirildak@firat.edu.tr
Received: 29.09.2024, Accepted: 28.10.2024

structures within the data, allowing for efficient model training on large amounts of unlabeled data [14],[19].

SSL can be considered a subfield of unsupervised learning since it does not involve manual labeling. However, when viewed within a narrower framework, unsupervised learning generally aims to uncover specific data patterns such as clustering, community discovery, or anomaly detection, whereas SSL targets extracting information from data based on the fundamental principles of supervised learning [14]. Figure 1 clearly illustrates the differences between these two approaches [20].

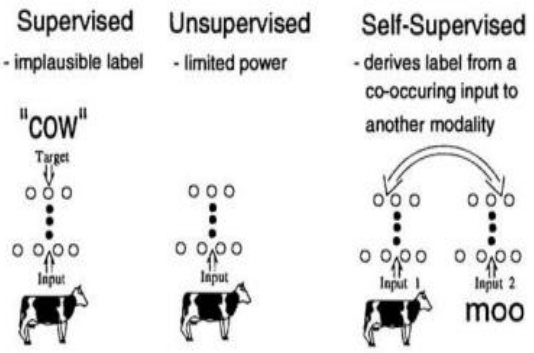

Figure 1. An Example of Supervised, Unsupervised, and Self-Supervised Learning.

Our main contributions in this study are given as follows.

- In the study, high success was achieved in the classification of unlabeled brain tumor images using the SimCLR-based SSL model. This approach effectively used unlabeled data and reduced the need for manual labeling.
- The proposed model achieved better results compared to other SSL techniques with high performance values such as 99.35% c_acc and 96.31% p_acc. This shows that the model is effective in medical image analysis.
- By using 6128 of the total 7671 images as unlabeled, a significant saving was achieved in the data labeling
- process and the need for manual labeling was minimized.
- By comparing different SSL techniques such as Barlow Twins, NnCLR and SimCLR, it was shown that the SimCLR-based model was superior. These comparisons are an important contribution in terms of evaluating the effectiveness of SSL techniques in medical image classification.
- The study showed that the SSL approach has a wide application potential, especially in areas such as medical image analysis where limited labeled data is available. This method can provide more efficient and faster medical image classification by reducing the need for expert knowledge.

2. Material and Method

2.1. Material

Although labels can be easily obtained through crowd sourcing from datasets, this method is limited in medical imaging because it requires expert knowledge. Therefore, this study was conducted to classify unlabeled data using the SSL technique with brain tumor images from medical images.

The brain is an organ that controls vital systems and tissues in the human body, such as hormonal regulation, memory, and reasoning. Brain tumors occur due to the abnormal proliferation of brain cells. Tumors, which are categorized as benign or malignant, increase intracranial pressure, complicating the control of vital systems and potentially leading to the patient's death in advanced stages. As with all types of cancer, early diagnosis and treatment increase survival rates for brain tumors. Changes in the brain can be detected using medical imaging techniques such as computed tomography and magnetic resonance imaging (MRI). The brain MRI images used in this study consist of four classes. These classes are specified as "glioma, meningioma, pituitary, and no_tumor."

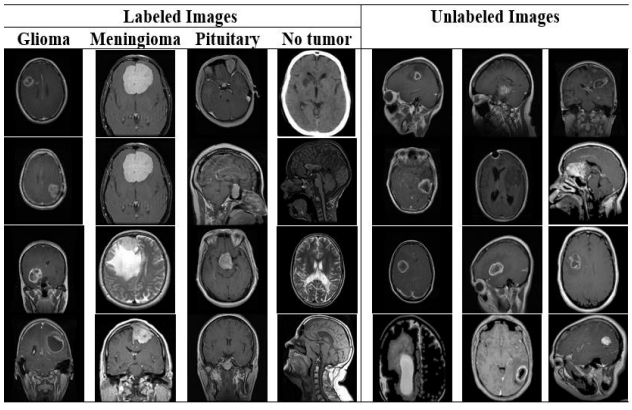

Figure 2. Some Labeled and Unlabeled Images Containing Brain Tumor Images.

In this study, three different datasets containing brain MRI images were used. The first dataset includes a total of 1311 MRI images, consisting of 300 Pituitary images, 306 Meningioma images, 300 Glioma images, and 405 No Tumor

images [21]. The second dataset contains a total of 3264 MRI images, comprising 901 Pituitary images, 937 Meningioma images, 926 Glioma images, and 500 No Tumor images [22]. The third dataset used contains a total of 3096 MRI images, including 844 Pituitary images, 913 Meningioma images, 901 Glioma images, and 438 No Tumor images [23]. To test the developed networks, the brain MRI datasets from three different sources were mixed and split into 1235 training data, 6128 unlabeled data, and 308 test data. Sample brain MRI images are shown in Figure 2.

2.2. Method

In this study, a SimCLR-based model is proposed for training on limited datasets with a small number of images. The performances of SimCLR [24], Barlow Twins [25] and NnCLR [26] techniques were also analyzed by examining these methods.

SimCLR, Barlow Twins, and NnCLR methods use twin networks. These networks aim to minimize the network error for representations of data belonging to the same class. Figure 3 (a) provides an example of a twin network architecture. The twin networks share the same network weights and attempt to learn to produce a minimum distance value for different samples belonging to the same class. This situation is the opposite for samples belonging to different classes. Figure 3 (b) illustrates this situation in detail for sample data from the MNIST dataset. The network error is calculated using methods like contrastive loss, and the network is trained.

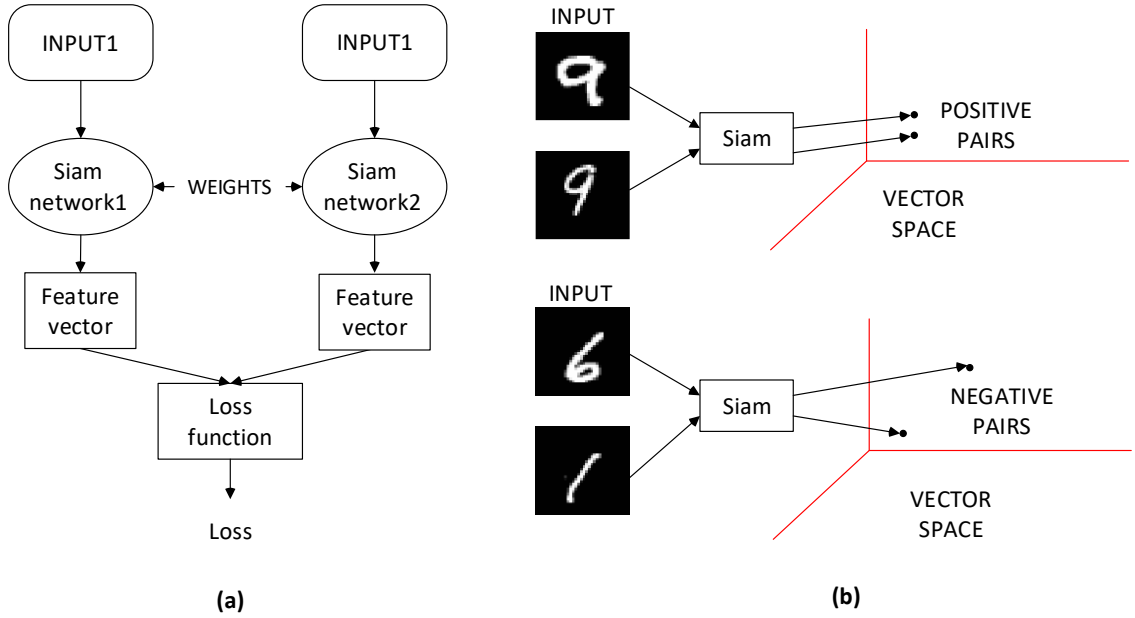

Figure 3. (a) Twin Network Architecture, (b) Positive and Negative Examples of Twin Networks in Vector Space

2.2.1. SimCLR

SimCLR fundamentally utilizes twin networks. These networks learn unlabeled data from datasets lacking sufficient amounts of data through classic data augmentation in four stages [24]. Figure 4 presents a schematic representation of the SimCLR method.

In the first stage of the SimCLR method, unlabeled data is augmented to create an increased data pool for each sample using classic data augmentation techniques (random resizing, random cropping, and adding Gaussian blur noise). In the second stage, the encoder network $f(.)$ obtains feature vectors for these augmented images x_i and x_j. In the third stage, a projection operation $g(.)$ is applied. At the end of this process, the contrastive loss value for the vectors z_i and z_j is calculated. The contrastive loss is given by the following equation.

$$l_{i,j} = -log \frac{exp\left(sim\left(z_i, z_j\right)/\tau\right)}{\sum_{k-1,indicator[k\neq i]}^{2N} exp\left(sim\left(z_i, z_j\right)/\tau\right)} \quad (1)$$

Here, N is the number of samples, and τ is the temperature parameter. The indicator function is defined as $\{Eğer\ [k \neq i]\ ise\ 1\ \}$. When calculating the loss, the contrastive loss is computed based on the cosine similarity between the selected number of positive data samples. The proposed model is trained

according to the backpropagation algorithm by taking the partial derivatives of the contrastive loss method.

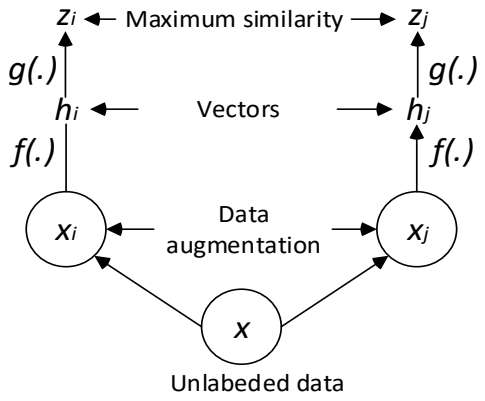

Figure 4. Schematic Representation of the SimCLR Method

2.2.2. Barlow twins

Barlow twins [25] is an innovative Contrastive Learning (CL) model that aims to perform classification on datasets with limited data using a self-supervised learning strategy with twin networks. This method generates augmented images T for all images in the sampled batch X. These images are provided as input in pairs y^a and y^b and y^a and y^b to the deep learning model f with parameters θ. The output of this model consists of feature vectors z^a and z^b. These vectors are assumed to be mean-centered over the batch size, resulting in an average output of 0 for each unit across the batch. The loss function of the Barlow Twins method is shown below.

$$L_{BT} \triangleq \sum_{\hat{1}} (1 - C_{ii}) + \lambda + \sum_{i} \sum_{j \neq i} C_{ij}^2 \qquad (2)$$

Here, λ is a positive constant that adjusts the importance of the first and second terms of the loss. C is the cross-correlation matrix calculated between the outputs of the twin networks over the batch size. This matrix is constructed according to the following equation.

$$C_{ij} \triangleq \frac{\sum_b z_{b,i}^A z_{b,j}^B}{\sqrt{\sum_b \left(z_{b,i}^A\right)^2} \sqrt{\sum_b \left(z_{b,j}^B\right)^2}} \qquad (3)$$

Here, b represents the batch samples. i, j are the vector dimensions of the network outputs. C has the output dimension of the network and takes values ranging from -1 (perfect anti-correlation) to 1 (perfect correlation) [25].

The objective function of the Barlow Twins method resembles the INFONCE method [27]. However, it stands out because it does not require a large number of negative samples and works effectively with high-dimensional vectors.
After calculating the Barlow Twins loss, the method trains the twin network according to the backpropagation algorithm.

2.2.3. NnCLR

Developed based on the SimCLR method, this approach is a modern self-supervised learning architecture that uses twin networks. The NnCLR method [26] employs the nearest neighbor clustering technique to increase the number of latent representations and obtain more diverse positive pairs rather than single positive examples [26]. This necessitates maintaining a vector support set that represents the entire data distribution. Figure 5 presents a schematic representation of the NnCLR algorithm.

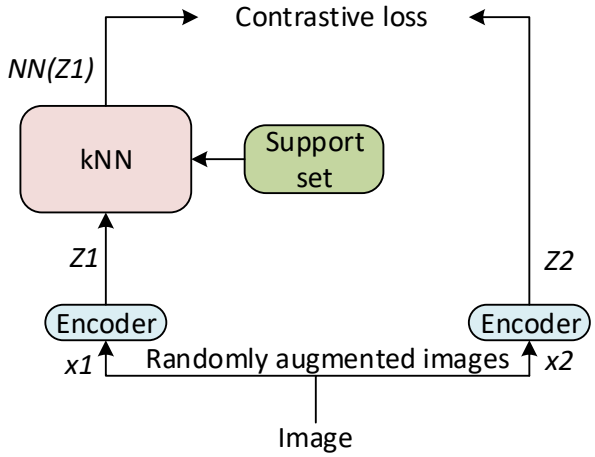

Figure 5. Schematic Representation of the NnCLR Method

SimCLR uses two augmented images z_i and $z_,^+$to create a positive pair. In contrast, NnCLR proposes using the nearest neighbors of z_i from the Q support set to form positive pairs. Similar to SimCLR, negative pairs are applied to the loss function in mini-batches. The loss function of the NnCLR algorithm is provided below.

$$L_i^{NnCLR} = -log \frac{exp(NN(z_i, Q) \cdot z_i^+ / \tau)}{\sum_k^n exp\left(NN(z_i, Q) \cdot z_i^+ / \tau\right)} \qquad (4)$$

2.2.4. Proposed Model

The overall structure of the proposed model is presented in Figure 6. The proposed model consists of the Encoder, Projection Head, and Classification stages. The model takes labeled and unlabeled images as input, and the Encoder module extracts feature maps. The Projection Head transforms the features extracted in the Encoder stage into a different space, creating similarity matrices between unlabeled and labeled data. In the Classification stage, the similarity matrices obtained in the Projection Head are used to predict which class the data may belong to.

In the Encoder stage, the input images undergo two convolution (Conv2D) operations followed by MaxPooling2D operations sequentially, repeated three times. The obtained features are then flattened into a vector using the Flatten operation and processed through three Dense layers. In the Conv2D operations, the number of filters (f) is set to 16, 32, and 64, with a filter size (kernel size) of 3x3. The activation function used after the Conv2D operations is ReLU. The Conv2D operation extracts feature maps from the images, while the MaxPooling2D operation reduces dimensionality by eliminating unnecessary features.

The Projection Head stage consists of three consecutive Dense layers. In these layers, the number of neurons is set to 256, 128, and 64, respectively. Additionally, the activation function used in each Dense layer is ReLU. The SimCLR loss function is employed for training the proposed Encoder and Projection architecture.

The Classification stage also consists of three consecutive Dense layers, with the number of neurons set to 256, 128, and 4, respectively. The activation function used in the first two Dense layers is ReLU. Categorical CrossEntropy is utilized for training the Classification module. The Categorical CrossEntropy (CE) cost function is as follows [28].

$$L_{CE} = -\sum_{i=1}^{N} y_i \,.\, log\, \hat{y}_i \tag{5}$$

Here, N represents the number of classes. y_i denotes the true classes, while $\hat{y}_i$ represents the predicted class.

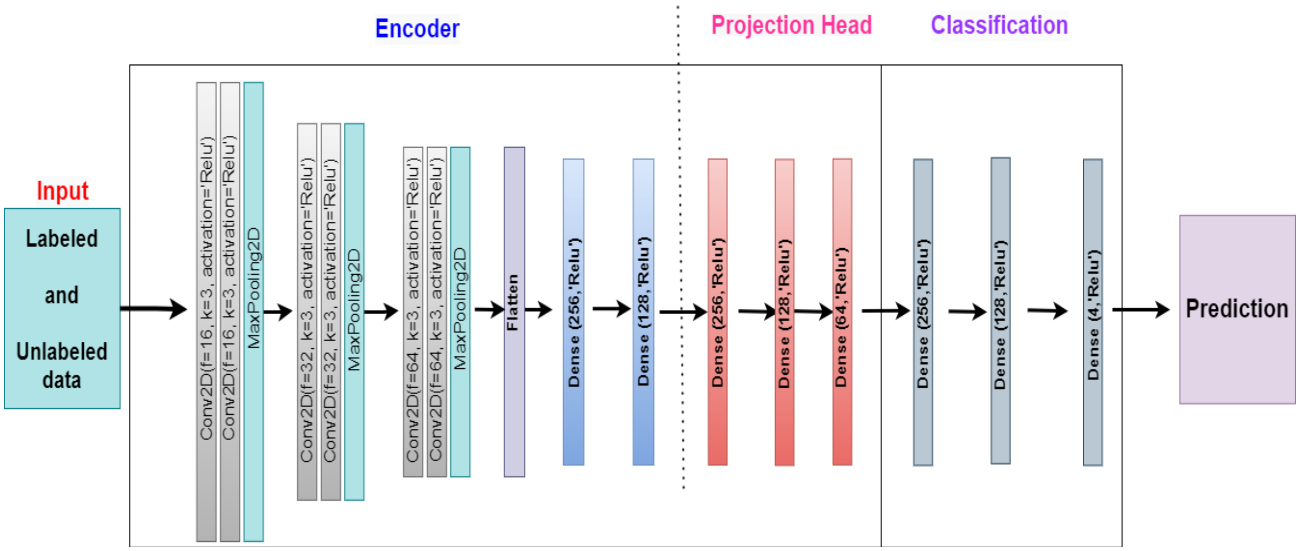

Figure 6. Overall Structure of the Proposed Model.

3. Results and Discussion

In this study, a SimCLR-based model was proposed to enhance the classification performance of unlabeled images. Three datasets containing brain tumor images were used, specifically comprising "pituitary," "meningioma," and "glioma" types, along with non-tumor images. A total of 7671 images were included in the datasets, out of which 6128 were designated as unlabeled data, while 1235 images were allocated for training and 308 for testing. The proposed model was trained using both labeled and unlabeled data.

For the training of the proposed model, the Adam optimization algorithm was employed, with SimCLR Loss and Categorical Crossentropy as the cost functions. The images were trained at a resolution of 96x96 over 100 epochs, with a temperature parameter τ set to 0.1. Data augmentation has been applied using the RandomFlip ("horizontal") method. This technique increases data diversity, allowing the model to generalize better. The

performance of the models is based on the Accuracy metric. This metric is given below:

$$Accuracy = \frac{TP + TN}{TP + TN + FP + FN} \quad (6)$$

Where, TP denotes the true-positive value, TN stands for the true-negative value, FP refers to the false-positive value, and FN indicates the false-negative value.

In the initial experimental study, the performance of the proposed model was compared to that of the SimCLR model, and the results are presented in Table 1. Additionally, the accuracy and loss graphs of the models are displayed in Figure 7. p_acc represents the accuracy of the classifier output, c_acc denotes the accuracy of comparative learning, r_acc indicates correlation accuracy, and val_p_acc reflects the test accuracy.

Table 1. Test Results of the Proposed Model vs. SimCLR.

Model	c_acc (%)	p_acc (%)	r_acc (%)	val_p_acc (%)
SimCLR	99.28	58.86	00.78	54.87
Proposed Model	**99.35**	**96.31**	**57.76**	**72.40**

The findings indicate that the proposed model achieved a comparative accuracy (c_acc) of 99.35%, a classification accuracy (p_acc) of 96.31%, a correlation accuracy (r_acc) of 57.76%, and a validation accuracy (val_p_acc) of 72.40%. These results demonstrate a significant improvement over the SimCLR model, underscoring the effectiveness of the proposed self-supervised learning approach in classifying unlabeled images. The substantial gains in accuracy metrics suggest that the model can efficiently leverage unlabeled data, enhancing performance in medical image classification tasks.

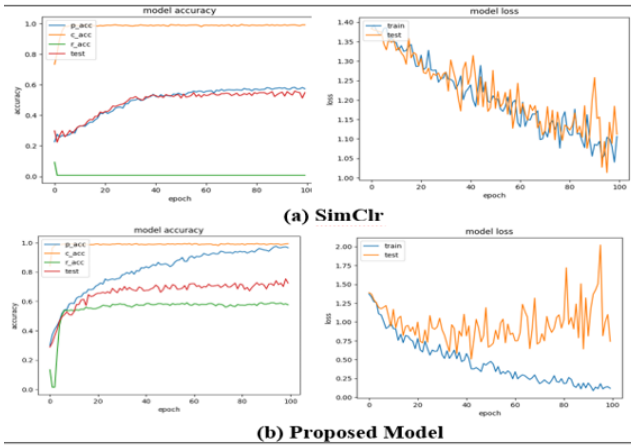

Figure 7. Accuracy and Loss Graphs of SimCLR and Proposed Model. (a) SimCLR Accuracy and Loss Graphs, (b) Proposed Model Accuracy and Loss Graphs.

This figure (Figure 7) illustrates the performance comparison between the SimCLR model and the proposed model. The accuracy and loss metrics for both models are displayed, providing insight into their training dynamics and overall effectiveness in classifying the datasets. The proposed model exhibits superior performance, as indicated by higher accuracy and lower loss across the training epochs.

The findings presented in this table summarize the performance metrics of the models employed in this study. Upon reviewing the results, it is evident that the proposed model predicts with significantly higher accuracy compared to the other models. This suggests that the incorporation of the self-supervised learning technique, particularly through the SimCLR framework, has contributed to enhanced classification performance in the context of brain tumor imaging.

Table 2. Test results of the models

Model	c_acc (%)	p_acc (%)	r_acc (%)	val_p_acc (%)
Barlow twins	98.65	56.63	35.94	53.25
NnCLR	98.36	62.36	36.26	58.12
SimCLR	99.28	58.86	00.78	54.87
Proposed Model	**99.35**	**96.31**	**57.76**	**72.40**

Accuracy and loss graphs of the models during training are presented in Figure 8. Additionally, the accuracy and loss graphs of the Barlow Twins and NnCLR models are shown in Figure 9. When examining the accuracy graph (a) in Figure 8, we can say that the proposed model demonstrates more stable and higher accuracy throughout the training.

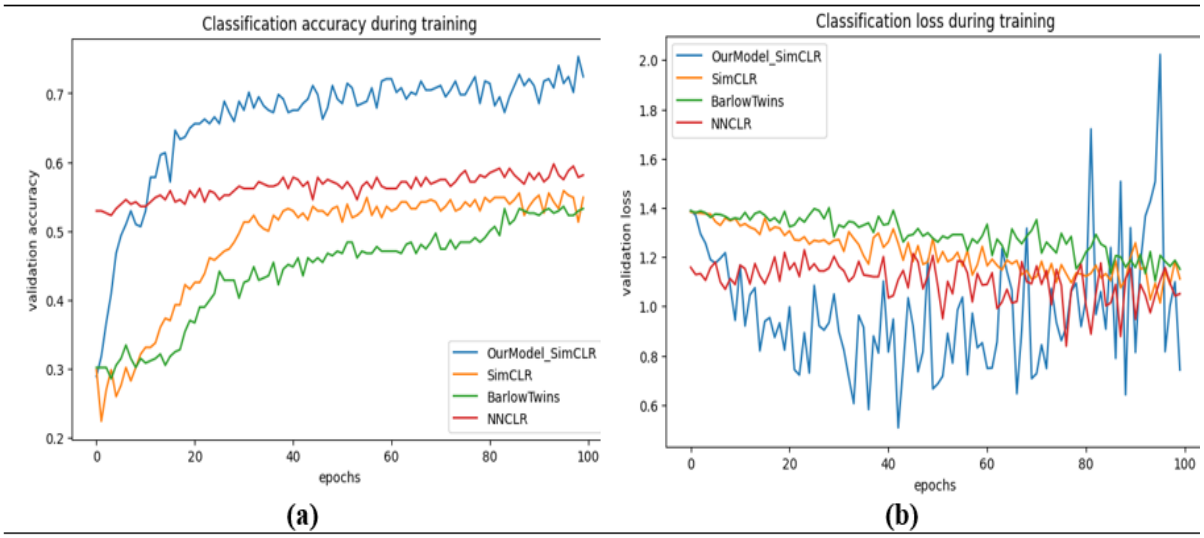

Figure 8. Accuracy (a) and loss (b) graphs of the models.

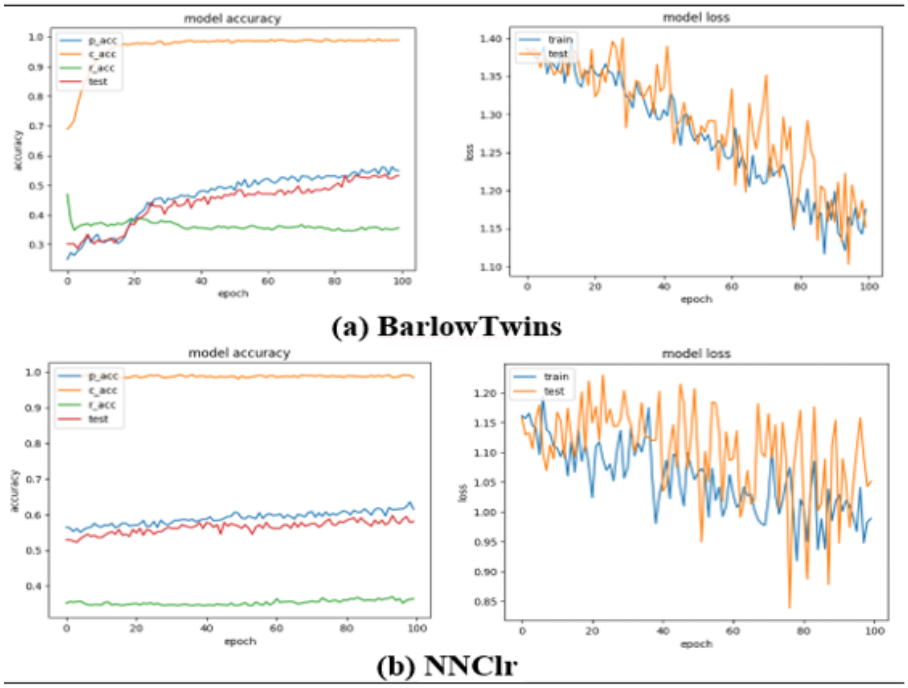

Figure 9. Accuracy and loss graphs of the BarlowTwins and NnCLR models. (a) BarlowTwins, (b) NnCLR model graphs

4. Conclusion and Suggestions

In this study, a SimCLR-based model was proposed using self-supervised learning (SSL) techniques to enhance the classification performance of unlabeled brain tumor images. The research was conducted on three types of brain tumors: pituitary, meningioma, and glioma, as well as non-tumor images. A dataset consisting of a total of 7,671 images was used, of which 6,128 were designated as unlabeled data, while the remaining images were utilized for training and testing. The proposed model was trained with both unlabeled and labeled data, effectively reducing the need for expert knowledge in medical imaging and minimizing the requirement for manual labeling.

As a result of performance analysis, it was observed that the proposed model achieved significant improvements compared to the SimCLR model, with values of 99.35% c_acc, 96.31% p_acc, 57.76% r_acc, and 72.40% val_p_acc. These findings demonstrate the effective utilization of unlabeled data through the SSL technique. It was concluded that this approach holds great potential for broader applications, especially in fields such as medical image analysis, where the labeled dataset is limited.

Contributions of the authors

Fırıldak: conceptualization, data collection, formal analysis, visualization, software development, interpretation of results
Çelik: methodology, literature review, interpretation of results, writing-first draft, revision
Talu: project administration, conceptualization, methodology, formal analysis, supervision, revision

Conflict of Interest Statement

There is no conflict of interest between the authors.

Statement of Research and Publication Ethics

The study is complied with research and publication ethics.

References

[1] M. Toğaçar, N. Muzoğlu, B. Ergen, B. S. B. Yarman, and A. M. Halefoğlu, "Detection of COVID-19 findings by the local interpretable model-agnostic explanations method of types-based activations extracted from CNNs," *Biomed. Signal Process. Control*, vol. 71, p. 103128, Jan. 2022, doi: 10.1016/j.bspc.2021.103128.

[2] G. Celik, "Detection of Covid-19 and other pneumonia cases from CT and X-ray chest images using deep learning based on feature reuse residual block and depthwise dilated convolutions neural network," *Appl. Soft Comput.*, vol. 133, p. 109906, Jan. 2023, doi: 10.1016/j.asoc.2022.109906.

[3] E. Başaran, "A new brain tumor diagnostic model: Selection of textural feature extraction algorithms and convolution neural network features with optimization algorithms," *Comput. Biol. Med.*, vol. 148, p. 105857, Sep. 2022, doi: 10.1016/j.compbiomed.2022.105857.

[4] G. Çelik and M. F. Talu, "A new 3D MRI segmentation method based on Generative Adversarial Network and Atrous Convolution," *Biomed. Signal Process. Control*, vol. 71, p. 103155, Jan. 2022, doi: 10.1016/j.bspc.2021.103155.

[5] S. Altun Güven and M. F. Talu, "Brain MRI high resolution image creation and segmentation with the new GAN method," *Biomed. Signal Process. Control*, vol. 80, p. 104246, Feb. 2023, doi: 10.1016/j.bspc.2022.104246.

[6] Z. Bozdag and M. F. Talu, "Pyramidal position attention model for histopathological image segmentation," *Biomed. Signal Process. Control*, vol. 80, p. 104374, Feb. 2023, doi: 10.1016/j.bspc.2022.104374.

[7] G. Celik and E. Başaran, "Proposing a new approach based on convolutional neural networks and random forest for the diagnosis of Parkinson's disease from speech signals," *Appl. Acoust.*, vol. 211, p. 109476, Aug. 2023, doi: 10.1016/j.apacoust.2023.109476.

[8] S. Mavaddati, "Voice-based age, gender, and language recognition based on ResNet deep model and transfer learning in spectro-temporal domain," *Neurocomputing*, vol. 580, p. 127429, May 2024, doi: 10.1016/j.neucom.2024.127429.

[9] M. A. Islam, M. Z. H. Majumder, M. A. Hussein, K. M. Hossain, and M. S. Miah, "A review of machine learning and deep learning algorithms for Parkinson's disease detection using handwriting and voice datasets," *Heliyon*, vol. 10, no. 3, p. e25469, Feb. 2024, doi: 10.1016/j.heliyon.2024.e25469.

[10] R. B. Rahman, S. A. Tanim, N. Alfaz, T. E. Shrestha, M. S. U. Miah, and M. F. Mridha, "A comprehensive dental dataset of six classes for deep learning based object detection study," *Data Br.*, vol. 57, p. 110970, Dec. 2024, doi: 10.1016/j.dib.2024.110970.

[11] B. Ganga, L. B. T., and V. K. R., "Object detection and crowd analysis using deep learning techniques: Comprehensive review and future directions," *Neurocomputing*, vol. 597, p. 127932, Sep. 2024, doi: 10.1016/j.neucom.2024.127932.

[12] K. Kantor and M. Morzy, "Machine learning and natural language processing in clinical trial eligibility criteria parsing: a scoping review," *Drug Discov. Today*, vol. 29, no. 10, p. 104139, Oct. 2024, doi: 10.1016/j.drudis.2024.104139.

[13] A. Montejo-Ráez, M. D. Molina-González, S. M. Jiménez-Zafra, M. Á. García-Cumbreras, and L. J. García-López, "A survey on detecting mental disorders with natural language processing: Literature review, trends and challenges," *Comput. Sci. Rev.*, vol. 53, p. 100654, Aug. 2024, doi: 10.1016/j.cosrev.2024.100654.

[14] L. Chen, P. Bentley, K. Mori, K. Misawa, M. Fujiwara, and D. Rueckert, "Self-supervised learning for medical image analysis using image context restoration," *Med. Image Anal.*, vol. 58, p. 101539, Dec. 2019, doi: 10.1016/j.media.2019.101539.

[15] A. Jaiswal, A. R. Babu, M. Z. Zadeh, D. Banerjee, and F. Makedon, "A Survey on Contrastive Self-Supervised Learning," *Technologies*, vol. 9, no. 1, p. 2, Dec. 2020, doi: 10.3390/technologies9010002.

[16] X. Liu *et al.*, "Self-supervised Learning: Generative or Contrastive," *IEEE Trans. Knowl. Data Eng.*, pp. 1–1, 2021, doi: 10.1109/TKDE.2021.3090866.

[17] I. Misra and L. van der Maaten, "Self-Supervised Learning of Pretext-Invariant Representations," in *2020 IEEE/CVF Conference on Computer Vision and Pattern Recognition (CVPR)*, Jun. 2020, pp. 6706–6716, doi: 10.1109/CVPR42600.2020.00674.

[18] Y. Wang, C. M. Albrecht, N. A. A. Braham, L. Mou, and X. X. Zhu, "Self-Supervised Learning in Remote Sensing: A review," *IEEE Geosci. Remote Sens. Mag.*, vol. 10, no. 4, pp. 213–247, Dec. 2022, doi: 10.1109/MGRS.2022.3198244.

[19] S. Shurrab and R. Duwairi, "Self-supervised learning methods and applications in medical imaging analysis: a survey," *PeerJ Comput. Sci.*, vol. 8, p. e1045, Jul. 2022, doi: 10.7717/peerj-cs.1045.

[20] V. R. de Sa, "Learning Classification with Unlabeled Data," in *Adv. Neural Inf. Process. Syst.*, pp. 112–119, 1994. [Online]. Available: https://dl.acm.org/doi/10.5555/2987189.2987204

[21] S. Gupta, "Brain MRI Scans for brain tumor classification," Accessed: Jan. 25, 2024. [Online]. Available: https://www.kaggle.com/datasets/shreyag1103/brain-mri-scans-for-brain-tumor-classification

[22] S. Bhuvaji, A. Kadam, P. Bhumkar, S. Dedge, and S. Kanchan, "Brain Tumor Classification (MRI)," Accessed: Jan. 12, 2024. [Online]. Available: https://www.kaggle.com/datasets/sartajbhuvaji/brain-tumor-classification-mri/data

[23] Thomas, "Brain tumors," Accessed: Jan. 18, 2024. [Online]. Available: https://www.kaggle.com/datasets/thomasdubail/brain-tumors-256x256?select=Data

[24] T. Chen, S. Kornblith, M. Norouzi, and G. Hinton, "A Simple Framework for Contrastive Learning of Visual Representations," Feb. 2020. [Online]. Available: http://arxiv.org/abs/2002.05709

[25] J. Zbontar, L. Jing, I. Misra, Y. LeCun, and S. Deny, "Barlow Twins: Self-Supervised Learning via Redundancy Reduction," Mar. 2021. [Online]. Available: http://arxiv.org/abs/2103.03230

[26] D. Dwibedi, Y. Aytar, J. Tompson, P. Sermanet, and A. Zisserman, "With a Little Help from My Friends: Nearest-Neighbor Contrastive Learning of Visual Representations," Apr. 2021. [Online]. Available: http://arxiv.org/abs/2104.14548

[27] A. van den Oord, Y. Li, and O. Vinyals, "Representation Learning with Contrastive Predictive Coding," Jul. 2018.

[28] J. C. Triana-Martinez, J. Gil-González, J. A. Fernandez-Gallego, A. M. Álvarez-Meza, and C. G. Castellanos-Dominguez, "Chained Deep Learning Using Generalized Cross-Entropy for Multiple Annotators Classification," *Sensors*, vol. 23, no. 7, p. 3518, Mar. 2023, doi: 10.3390/s23073518.